OPEN ACCESS

University of BRISTOL

Peer reviewed version

Link to published version (if available):
10.1177/0892705715598362

Link to publication record in Explore Bristol Research
PDF-document

University of Bristol - Explore Bristol Research
General rights

Analysis of the damage mechanisms in mixed-mode delamination of laminated composites using acoustic emission data clustering

Mohamad Fotouhi[1]*, Seyedali Sadeghi*, Meisam Jalalvand** and Mehdi Ahmadi*

*Non-destructive Testing Lab, Department of Mechanical Engineering, Amirkabir University of Technology, 424 Hafez Ave, 15914, Tehran, Iran.

** Advanced Composites Centre for Innovation and Science, University of Bristol, Bristol BS8 1TR, UK

Abstract

In this study, Acoustic Emission (AE) technique is concerned with an investigation of the delamination damage and time-to-failure mechanisms on this phenomenon in glass/epoxy composite laminates. Woven and unidirectional lay-ups were subjected to the Double Cantilever Beam (DCB), End Notch Flexure (ENF) and Mixed-Mode Bending (MMB) tests and the generated AE signals were captured. Discrimination of the AE events, caused by different types of the damage mechanisms, was performed using Wavelet Packet Transform (WPT) and Fuzzy Clustering Method (FCM) associated with a Principal Component Analysis (PCA). The FCM and WPT analyses showed that three dominant damage mechanisms are the origins of the AE signals in the tests. Furthermore, different interface lay-ups and different GII/GT modal ratio values indicate different time-to-failure mechanisms incidence. Additionally, scanning Electron Microscope (SEM) was employed to observe the damage mechanisms. The results showed that dominant damage mechanisms in all the specimens are matrix cracking and fiber-matrix debonding. Besides, some fiber breakage appeared during the tests, and the percentage of this damage mechanism in the unidirectional specimens and mode I condition was higher than those in the woven specimens and mode II. The comparison between the results of SEM observation and

---

[1] Corresponding author; Tel: (+98 21 6454 3431)　　　　　　Fax:+98 21 8871 2838
Email address: fotouhi.mohamad@gmail.com

obtained damage mechanisms using WPT and FCM showed an acceptable agreement. It was found that the presented methods can be established as an automated procedure in the classification process to improve the characterization and discrimination of damage mechanisms in the actual occurring modes of delamination in composite structures.

Introduction

Composite structures are extensively used as engineering structures which normally are subjected to complex loads. One of the main drawbacks of many advanced laminated composite structures is their susceptibility to delamination. Mode I, mode II and the combination of these pure modes are usually present in many real conditions of the delamination damage which may degrade the mechanical properties of laminated composites. Loading conditions and layup types are among effective factors in the delamination behavior. Consequently, a better understanding of the delamination in different loading conditions and lay-up variation is an essential research topic and could help to increase reliability and safety of the composite structures against initiation and growth of the delamination [1-2].

Different non-destructive methods have been utilized to detect delamination damage in composite materials. AE is known as an in situ and promising non-destructive technique for investigation of microscopic behavior of fiber matrix interface during delamination. AE

signal is a transient wave resulting from real-time and continuous monitoring of micro failures (e.g. matrix cracking, debonding of matrix from fiber and fiber failure) during delamination phenomenon [3-6].

Until now, some researchers discriminated the AE signatures of damage mechanisms in composite materials [7-12]. Their results showed that AE technique is a capable tool for characterization of damage mechanisms in thermoplastic and thermoset laminated composite materials. Most of these studies exploited AE parameters such as amplitude, count and energy for characterizing the damage mechanisms. Obtained results showed that the AE signals are distributed into distinct clusters. Furthermore, three dominant damage mechanisms (matrix-cracking, fiber-matrix debonding and fiber breakage) take place during delamination while these different damage mechanisms generate different AE parameters. Additionally, the achieved results specified that higher frequencies and amplitudes emerging in the tests were related to fiber breakage while lower ranges contributed to matrix cracking and fiber-matrix debonding damages [2, 8, 9, 10].

In order to obtain more reliable and accurate information for identification of damage mechanisms, pattern recognition algorithms and time frequency analyses were utilized as multivariable classification procedures of AE data. These methods made it possible to study the delamination damage mechanisms by simultaneous consideration of the various AE

features [13-16]. In another studies, [17-18] the combination of AE and mechanical information were used to recognize the behavior of damage mechanisms during delamination damage while notable results were achieved.

In this study, two powerful multivariable techniques of Fuzzy Clustering Method (FCM) and Wavelet Packet Transform (WPT) were utilized to investigate time to failure mechanisms generated during delamination damage. FCM is the combination of fuzzy concept and K-Mean method. This technique was used to classify AE signals by different researchers [19-22]. The results showed that this technique has good applicability for clustering the AE signals. Furthermore, this method can be applied to discriminate the AE events having high degree of overlapping in their parameters. WPT [23-26], one of the time–frequency distribution techniques, was employed in some studies to investigate the relationship between AE signals and damage sources. The results of this method clarified that this method and frequency analysis is efficient way for processing the AE signals of composite materials.

Up to now, several AE based studies were conducted regarding failure modes during propagation of delamination. However, the previously referenced studies were mostly on mode I fracture analysis while there is lack of studies related to the failure study of delamination during mode II and mixed mode types. Therefore, in this work, evaluation of

micro-cracking occurrence and identifying the type of damages are conducted when subjected to mode I, mode II and mixed-mode delamination tests. Two different types of glass/epoxy composite specimens including unidirectional and woven are chosen. In fact, the aim of this paper is to improve the investigation efficiency in discriminating various AE sources obtained during actual occurring modes of delamination damage. From this standpoint, WPT and FCM associated with Principal Component Analysis (PCA) were applied to identify the acoustic signatures of the damage mechanisms in real occurring modes of delamination. Six AE parameters including amplitude, frequency, etc. were used for the FCM based classification, while the energy criterion was utilized to analyze decomposed levels in WPT. The damage mechanisms were also observed using the SEM images for the purpose of verification. The procedure for damage recognition can clearly be seen in Figure 1.

Figure 1. The procedure for damage recognition.
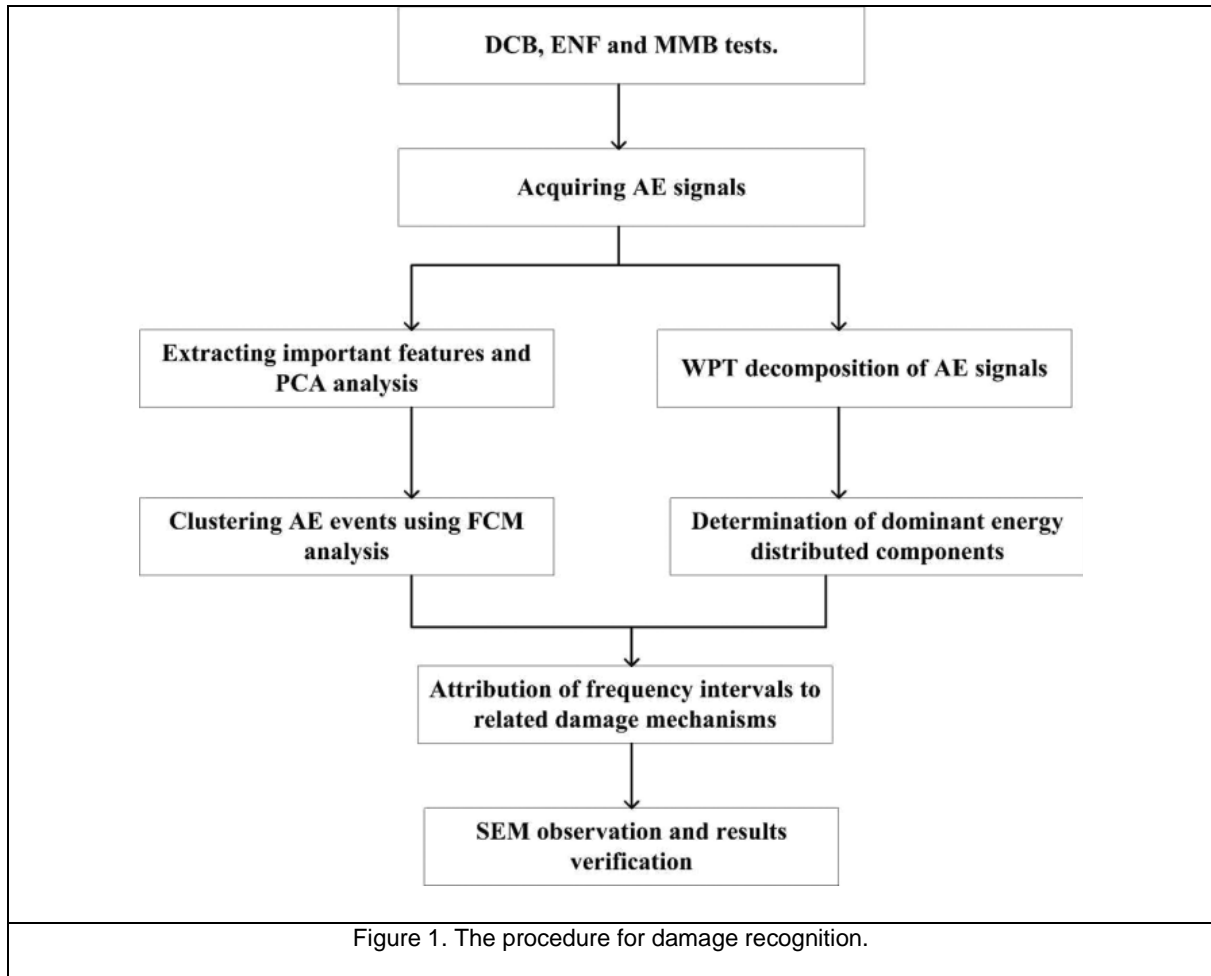
Experimental procedure

Material and specimen preparation

The experimental work was carried out on the epoxy resin reinforced by the E-glass unidirectional and woven fiber with the density of 1.46 g/cm^3, 500 g/m^2, and 303 g/m^2,

respectively. Two different interface types which were used for this study are specified in Table 1. The laminates were prepared by hand lay-up. The starter crack was formed by inserting a Teflon film with thickness of 20 μm at mid-plane during molding as an initial crack for delamination. As shown in figure 2, the laminated composite test specimens consist of a rectangular shape and uniform thickness (the fabrication tolerance for all the dimensional is about ± 0.1 mm).
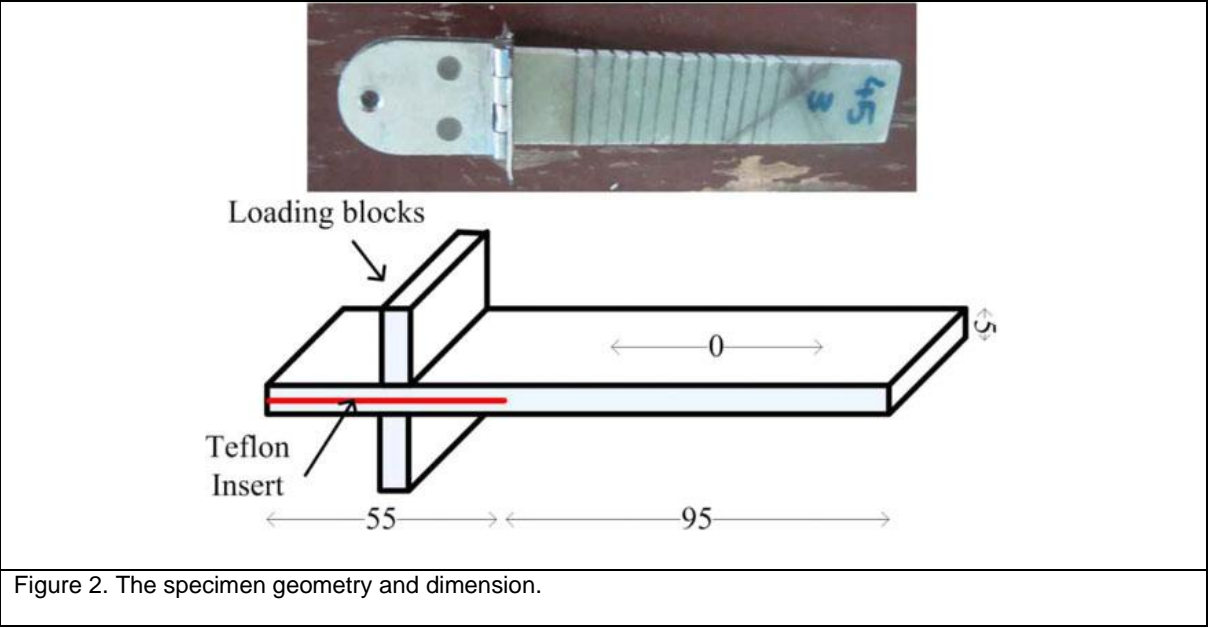

Figure 2. The specimen geometry and dimension.

Table 1. Specification of the investigated lay-ups for sample U1-U4 and W1-W4.

Name	Mid-plan	Lay up	Loading condition
U1	0, 0	$[0°]_{18}$	Mode I
U2	0, 0	$[0°]_{18}$	GII/GT =18%
U3	0, 0	$[0°]_{18}$	GII/GT =30%
U4	0, 0	$[0°]_{18}$	Mode II
W1	W-W	Woven	Mode I

W2	W-W	Woven	$G_{II}/G_T = 18\%$
W3	W-W	Woven	$G_{II}/G_T = 30\%$
W4	W-W	Woven	Mode II

Test procedure

DCB, ENF and MMB test apparatus, shown in Figure 3, were used to split the laminated specimens. In DCB setup, an upward force was applied to split end of the laminate to create mode I, whereas in ENF setup, a downward load was applied to the center of specimen to create Mode II. MMB is the combination of DCB and ENF in which the length of the lever arm can vary to change the GII/GT modal ratio values. In this paper, two different GII/GT modal ratio values were studied (see Table 1). Delamination tests were carried out at a temperature of 24°C at a constant displacement rate of 2mm/min. A properly calibrated universal tensile test machine was used while the load cell capacity of the test machine is 5000 N. The load and displacement were continuously measured and the crack length was visually observed.
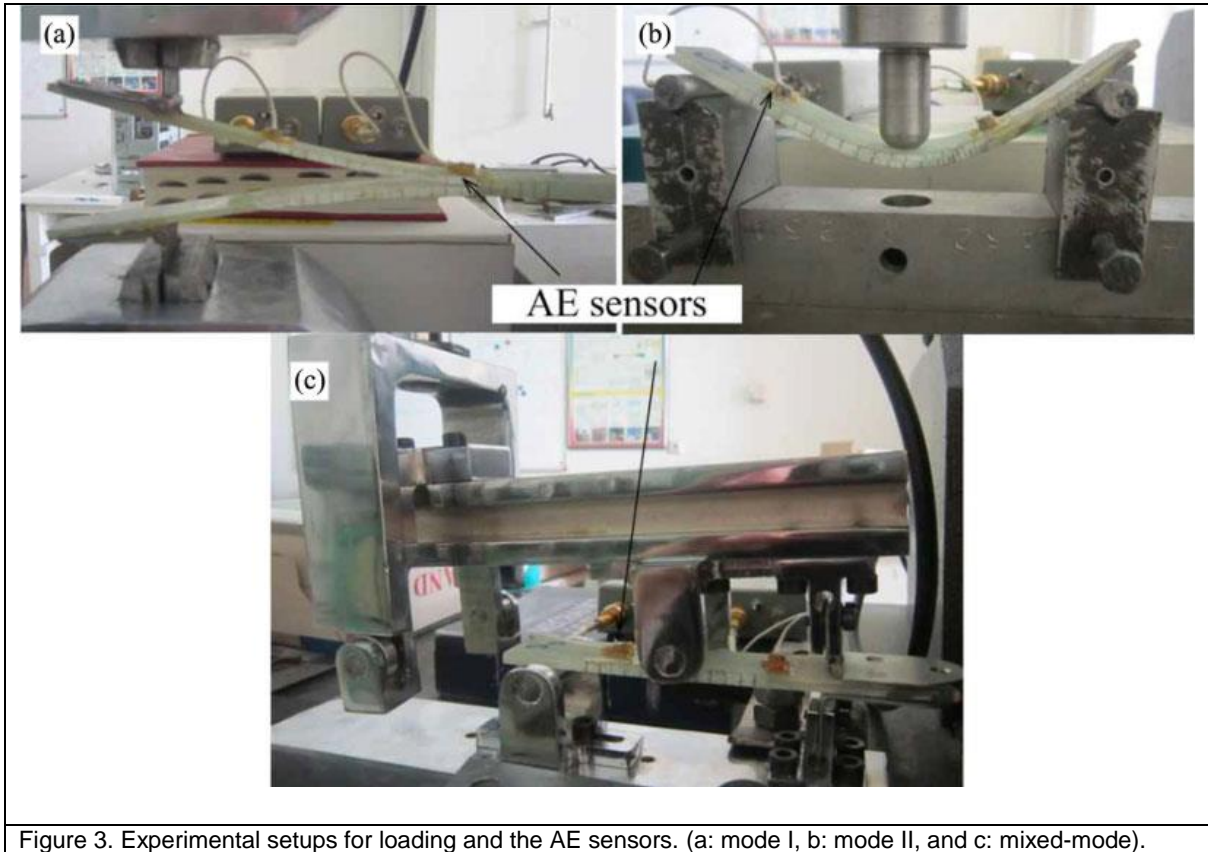
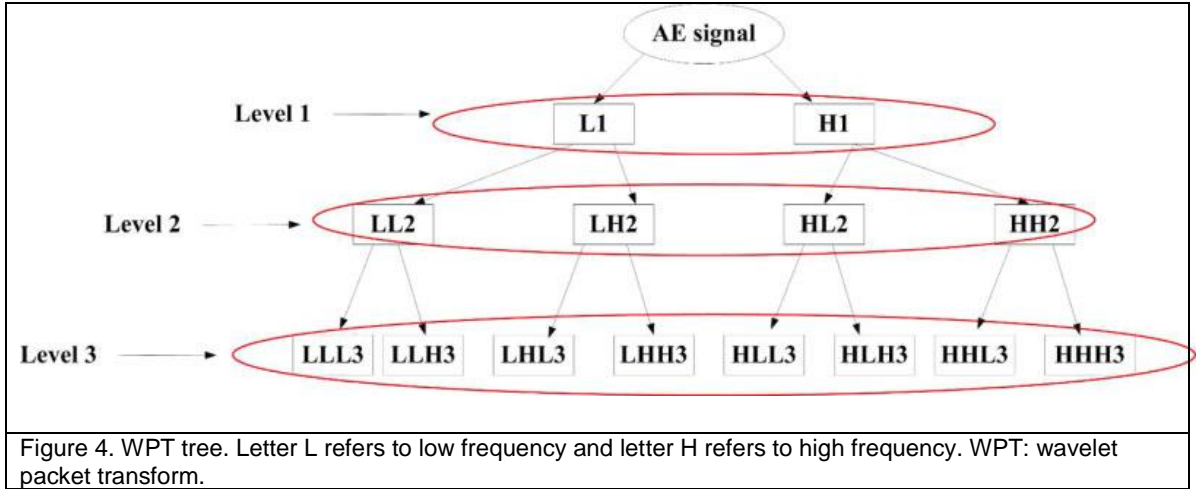Figure 3. Experimental setups for loading and the AE sensors. (a: mode I, b: mode II, and c: mixed-mode).

AE device

AE events were recorded by using Acoustic emission software AEWin and a data acquisition system PAC PCI-2 with a maximum sampling rate of 40 MHz. PICO, a broadband, resonant-type, single-crystal piezoelectric transducer from PAC used as the AE sensor. The sensor has a resonance frequency of 453.12 kHz and an optimum operating range of 100–750 kHz. So as to provide good acoustic coupling between the specimen and

the sensor, the surface of the sensor was covered with grease. The signal was detected by the sensor and enhanced by a 2/4/6-AST preamplifier. The gain selector of the preamplifier was set to 40 dB. The test sampling rate was 1 MHz with 16 bits of resolution between 10 and 100 dB. Prior to the damage check, the data acquisition system was calibrated for each kind of the specimens, according to a pencil lead break procedure. This procedure enables the generation of the waves used for the device calibration at the specimen surface. At the same time, the velocity and attenuation of the AE waves were measured. The lead breakage operation was repeated several times at different locations between the sensors. After the calibration step, the AE signals were captured during mechanical testing. Signal descriptors, such as amplitude, duration, rise time, counts and energy, were calculated by the AE software (AEWin).

Wavelet-based Methodology

The theory of Wavelet is well documented in textbooks concerning multivariable data analysis [23-26], where the wavelet transform is represented as a suitable method for analyzing AE signals. In this study, WPT is employed [27-28] in which each signal is split into high-frequency and low-frequency components as shown in Figure 4. The number of components for level i is 2^i.

Figure 4. WPT tree. Letter L refers to low frequency and letter H refers to high frequency. WPT: wavelet packet transform.

The frequency ranges of the high and the low components are calculated from Equations (1a) and (1b), respectively, where f_s is the sampling rate and i is the number of decomposition level.

$$[\frac{1}{2}f_s 2^{-i}, \frac{1}{2}f_s 2^{-(i-1)}] \tag{1a}$$

$$[0, \frac{1}{2}f_s 2^{-i}] \tag{1b}$$

In this study, relative energy distribution at each level ($P_i^j(t)$) was exploited for characterization of failure modes which could be expressed in Equations 2-4 as follow:

$$P_i^j(t) = \frac{E_i^j(t)}{E_{Total}(t)} \qquad j = 1...2^i \tag{2}$$

$$E_i^j(t) = \sum_{\tau=t_0}^{t} \left(f_i^j(\tau)\right)^2 \tag{3}$$

$$E_{Total}(t) = \sum_i E_i^j(t) \tag{4}$$

Where $E_i^1...E_i^j$ express the energy components at level i, E_{Total} is the total energy of signal, $f(t)$ is an AE signal and $f_i^1...f_i^j$ are the components of ith level of the decomposed signal.

Principal Component Analysis (PCA)

The theory of PCA is well explained in textbooks expressing multivariable data analysis [19, 29]. Briefly introducing, PCA is a multivariate analysis tool commonly used for reducing dimensionality of a large dataset to enable better visualization and analysis of data [21]. Dimensional reduction is performed by transforming data to a new set of uncorrelated variables, i.e., the principal components. Indeed, PCA projects the data along the directions that describe maximum variance in the dataset.

The Fuzzy C-means clustering

FCM is a clustering procedure in which each input data belongs to some clusters with a degree that is defined by a membership grade [29]. Input data with some multidimensional space could be classified as specific numbers of different clusters, using FCM method. According to Equation 5, input data (P) is signified as n×m matrix.

$$P_{n \times m} = \begin{bmatrix} p_{11} & \cdots & p_{1m} \\ \vdots & \ddots & \vdots \\ p_{n1} & \cdots & p_{nm} \end{bmatrix} \tag{5}$$

Equation 6 is the mathematical express of the objective function intended for FCM clustering. The basic concept of the objective function is to minimize the Euclidian distance between each data in its cluster and cluster center, and to maximize the Euclidian distance between other cluster centers.

$$J(P;U,S) = \sum_{i=1}^{c} \sum_{r=1}^{m} (\gamma_{ir})^{\alpha} \|p_r - s_i\|_A^2 \tag{6}$$

$$S = [s_1, s_2, ..., s_c] \tag{7}$$

$$D_{irA}^2 = \|p_r - s_i\|_A^2 = (p_r - s_i)^T A (p_r - s_i) \tag{8}$$

$$\gamma_{ir} \in [0,1] \quad 1 \le i \le c, 1 \le r \le m \tag{9}$$

$$\sum_{i=1}^{c} \gamma_{ir} = 1 \quad 1 \le r \le m, \tag{10}$$

$$0 \prec \sum_{r=1}^{m} \gamma_{ir} \prec m, \quad 1 \le i \le c. \tag{11}$$

In the Equations 6-11, J is a fuzzy partition matrix of input data (P), S is cluster centers vector, D is a squared inner-product distance norm, $\alpha \in [1,\infty)$ is a fuzziness parameter of the clusters and γ is the membership value.

Simple Picard iteration, using the first-order conditions for stationary points of Equation 6, is known as the FCM algorithm [30]. This iteration procedure is the most well-known technique for minimization of the c-means function. In fact, it could be observed that if $D_{irA}^2 \succ 0, \forall i, r \ and \ \alpha \succ 1 \ then (U,S)$ may minimize Equation 6 only if the Equations 12-13 are satisfied.

$$\gamma_{ir} = \frac{1}{\sum_{j=1}^{c} \left(\dfrac{D_{irA}}{D_{jrA}} \right)^{\frac{2}{\alpha-1}}} \qquad 1 \le i \le c, 1 \le r \le m, \tag{12}$$

14

$$S_i = \frac{\sum_{r=1}^{m}(\gamma_{ir})^{\alpha} p_r}{\sum_{r=1}^{m}(\gamma_{ir})^{\alpha}} \qquad 1 \le i \le c$$

(13)

FCM procedures for classification of the AE data are stated bellow:

The input parameters, including data set (P), weighting exponent (α>1), number of clusters (1< c < m), termination tolerance (ε>0)) and norm-inducing matrix A, are selected [30]. Initial value such as $U^{(0)}$ is selected randomly, for the partition matrix (U). The following steps are reiterated for l= 1, 2, 3 …

Step 1: Using Equation 13, the cluster centers (S_i) are calculated.

Step 2: Using Equation 8, the distances $\left(D^2\right)$ are evaluated.

Step 3: The partition matrix is updated for $1 \le r \le m$.

If D_{irA} > 0 for all i = 1, 2, 3 …

$$\gamma_{ir}^{(l)} = \frac{1}{\sum_{j=1}^{c}\left(\frac{D_{irA}}{D_{jrA}}\right)^{\frac{2}{\alpha-1}}}$$

Otherwise

$$\gamma_{ik}^{(l)} = 0$$

The FCM iterates until $U^{(l)} - U^{(l-1)} \prec \varepsilon$

Results and discussion

The load and energy of the AE signals versus displacement for the specimens are shown in Figures 5 and 6. As can be seen, the plots trends are classified as 3 regions. This classification is because of the different delamination behavior in these regions. Region 1 is related to the free failure domain while regions 2 and 3 are associated with the initiation and propagation of the delamination.
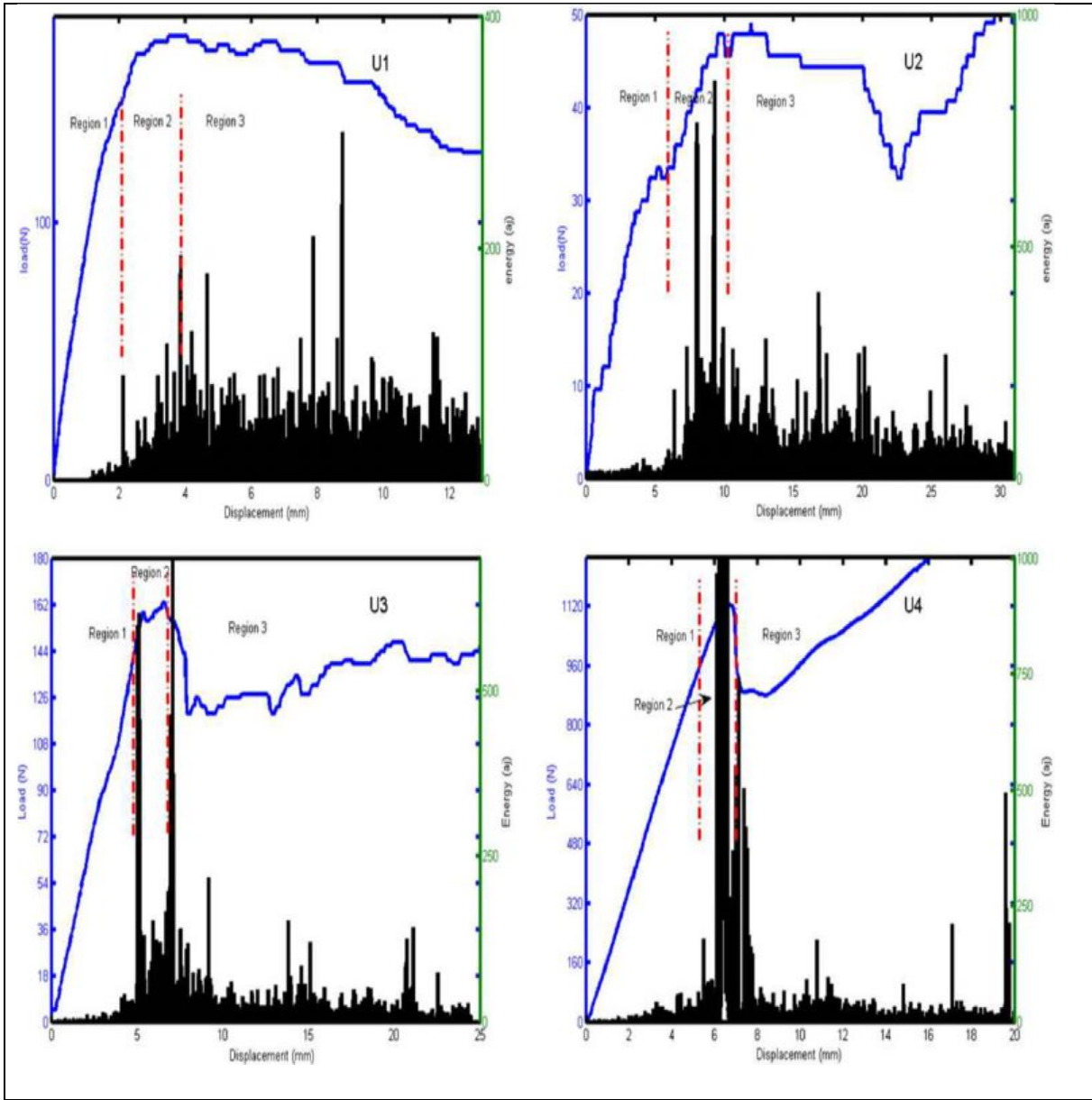
Figure 5. The load/time curves and AE energy distribution for the unidirectional specimens.
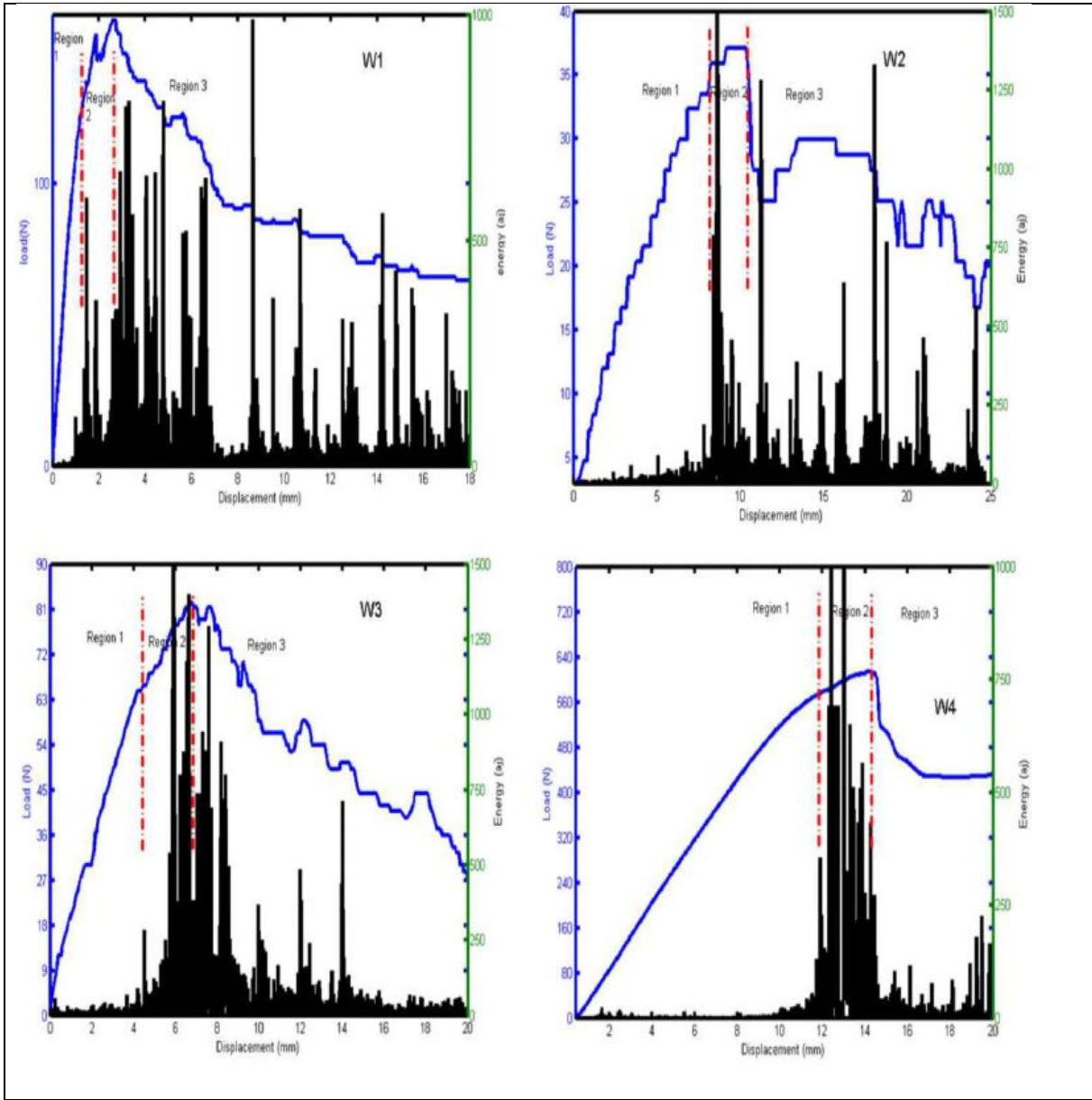
Figure 6. The load/time curves and AE energy distribution for the woven specimens.

There are some dissimilarity between the mechanical and AE behaviors in each region for the investigated specimens. As illustrated in Figures 5 and 6, the length of region 1 varies by changing the lay-up type and GII/GT modal ratio value. It can be observed that the mode I condition is more sensitive to the strain causing the delamination onset appears sooner compared to the other loading conditions. The distribution of AE events is also different in the investigated specimens. There is almost uniform distribution of the AE energy after the initiation stage in mode I. In fact, for pure mode I, the load increases continually until the maximum load. The load is then almost constant, but increasing of the GII/GT modal ratio value causes the distribution of the AE energies to be burst type. After the onset of delamination, the crack growth in mode I condition is stable, whereas the crack growth in mode II condition and the GII/GT values near mode II is unstable. In the mentioned modes, the load increases in a single stage until the maximum load, subsequently there is an instability appearance after the maximum load.

As previously discussed, there are different AE and mechanical behaviors in the investigated specimens. Variations in the AE events and mechanical behaviors reflect occurrence of different damage mechanisms. These differences are due to the different interface lay-ups and different loading conditions leading to the different damage

mechanisms. Waveforms of specimen U1 obtained from different regions along with the wave characteristics are shown in Figure 7.
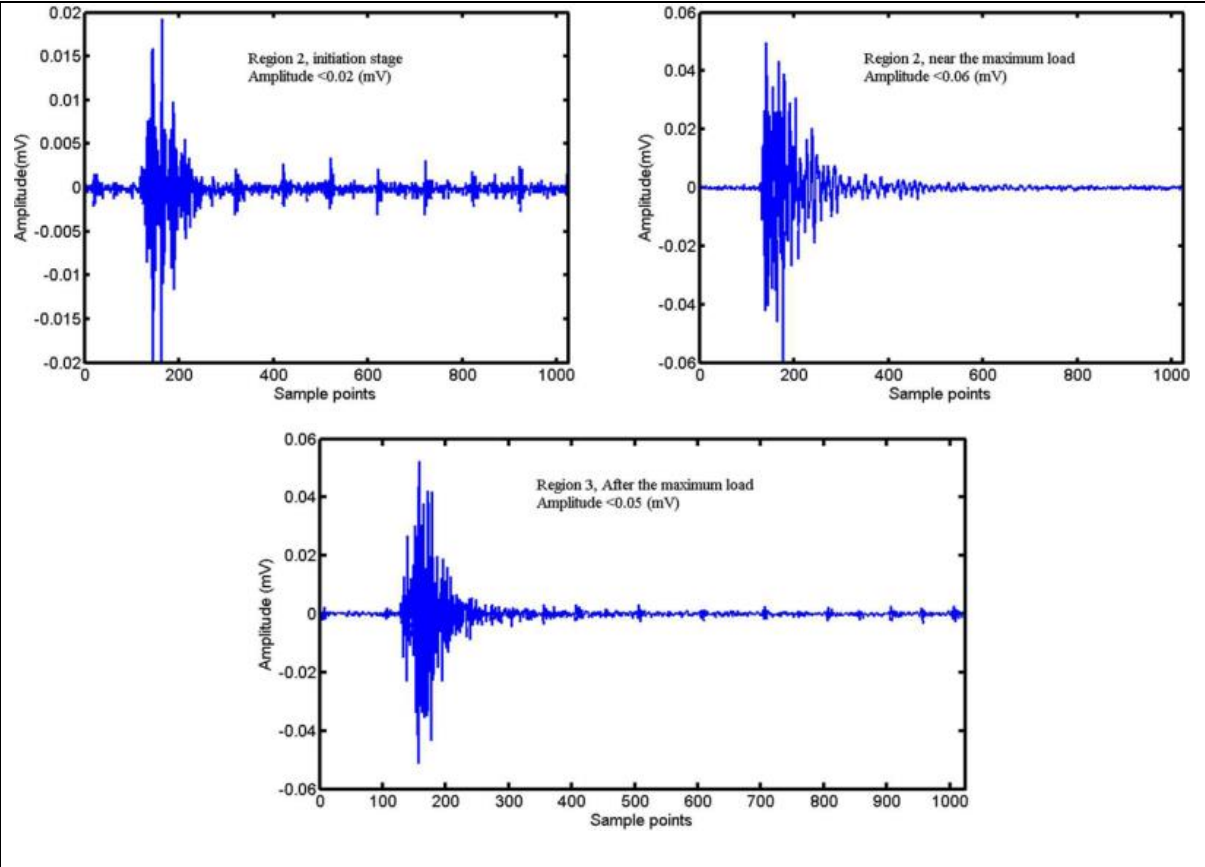

Figure 7. Waveforms of specimen U1 obtained from different regions.

Studying the recoded waveforms in time domain shows that the amplitude range of the detected waveforms varies as a result of different AE events in the introduced regions. The

reason for the generation of different types of waveforms could come from the different failure modes during propagation of delamination. A more extracted signatures description from the AE waveforms for identification of the damage mechanisms can be obtained by applying WPT and FCM associated with PCA methods.

Multivariable analysis

Multivariable analysis techniques including WPT and FCM associated with PCA are applied to discriminate time to failure mechanisms according to their AE patterns.

WPT results. WPT and Daubechies' wavelet family [24] were employed to analyze the AE signals. Each obtained AE signal is decomposed into three different levels. Entropy criteria [25] were also applied for deciding if certain decomposition is adequate or more levels are needed. The relative energy distribution of the AE signals for all components of the third level is then calculated from Equations 2 and 3. The summary of the WPT results are illustrated in Figure 8 and Table 2.
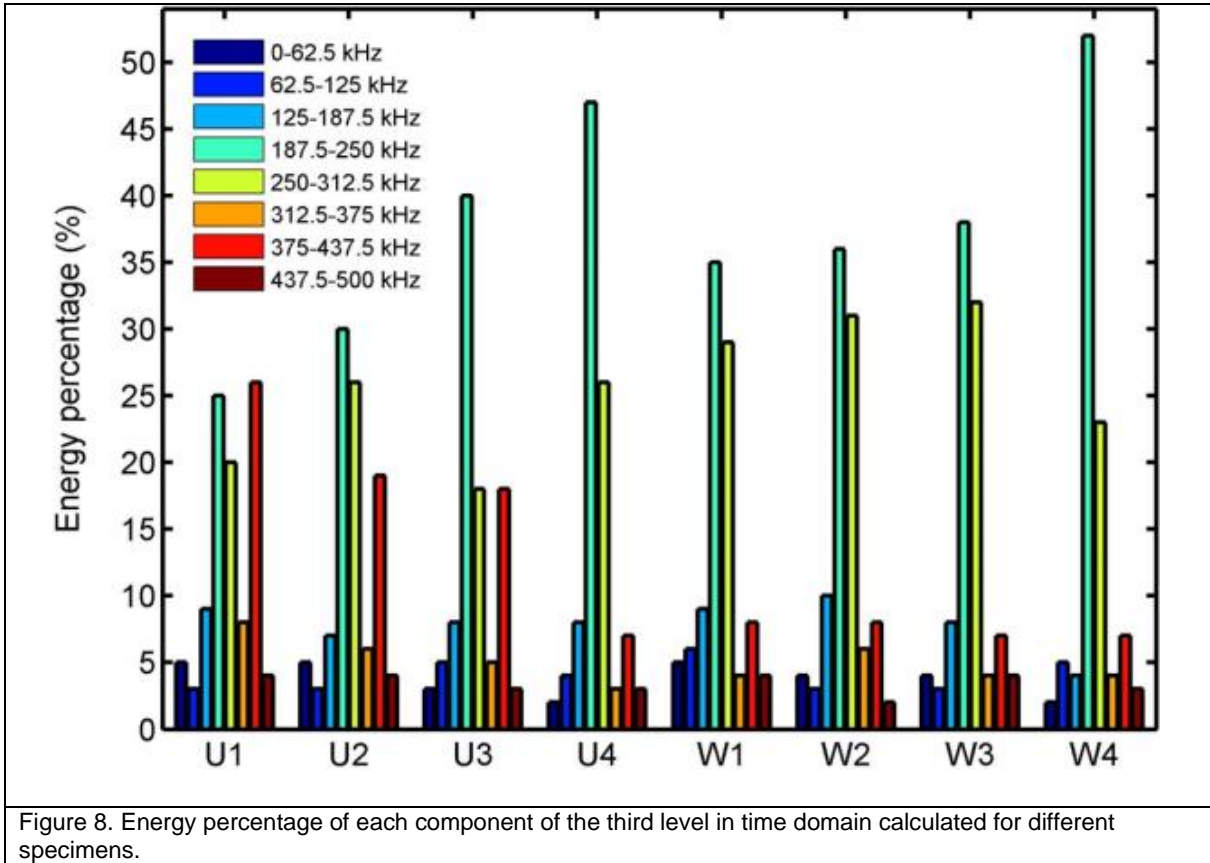
Figure 8. Energy percentage of each component of the third level in time domain calculated for different specimens.

Table 2. Summary of wavelet packet analysis for dominant components.

	specimen	Frequency ranges (kHz)		
		187.5-250	**250-312.5**	**375-437.5**
Energy Percentage (%)	U1	**25**	**20**	**26**
	U2	**30**	**26**	**19**
	U3	**40**	**18**	**18**
	U4	**47**	**26**	**7**
	W1	**35**	**29**	**8**

W2	**36**	**31**	**8**
W3	**38**	**32**	**7**
W4	**52**	**23**	**7**

As can be observed, the major portion of the AE energy is distributed in 3 dominant components (LHH3, HLL3 and HHL3) for the specimens. Approximately, more than 70% of the AE events are related to these three components. However, the energy distribution percentage at each one of these dominant components varies from one experimental condition to another (see Figure 8). Furthermore, it can be seen from Table 2 that the frequency range of components LHH3, HLL3 and HHL3 are 187.5-250 kHz, 250-312.5 kHz and 375-437.5 kHz, respectively.

FCM analysis. Six important features of the AE signals (amplitude, frequency, energy, count, rise time, duration) were employed for PCA analysis. The PCA results show that more than 80% of the total variance of the input data is related to the cumulative sum of the variances of the PCA (1) and PCA (2).

The PCA visualization of the FCM on the AE signals is shown in Figures 9 and 10 for all the specimens.
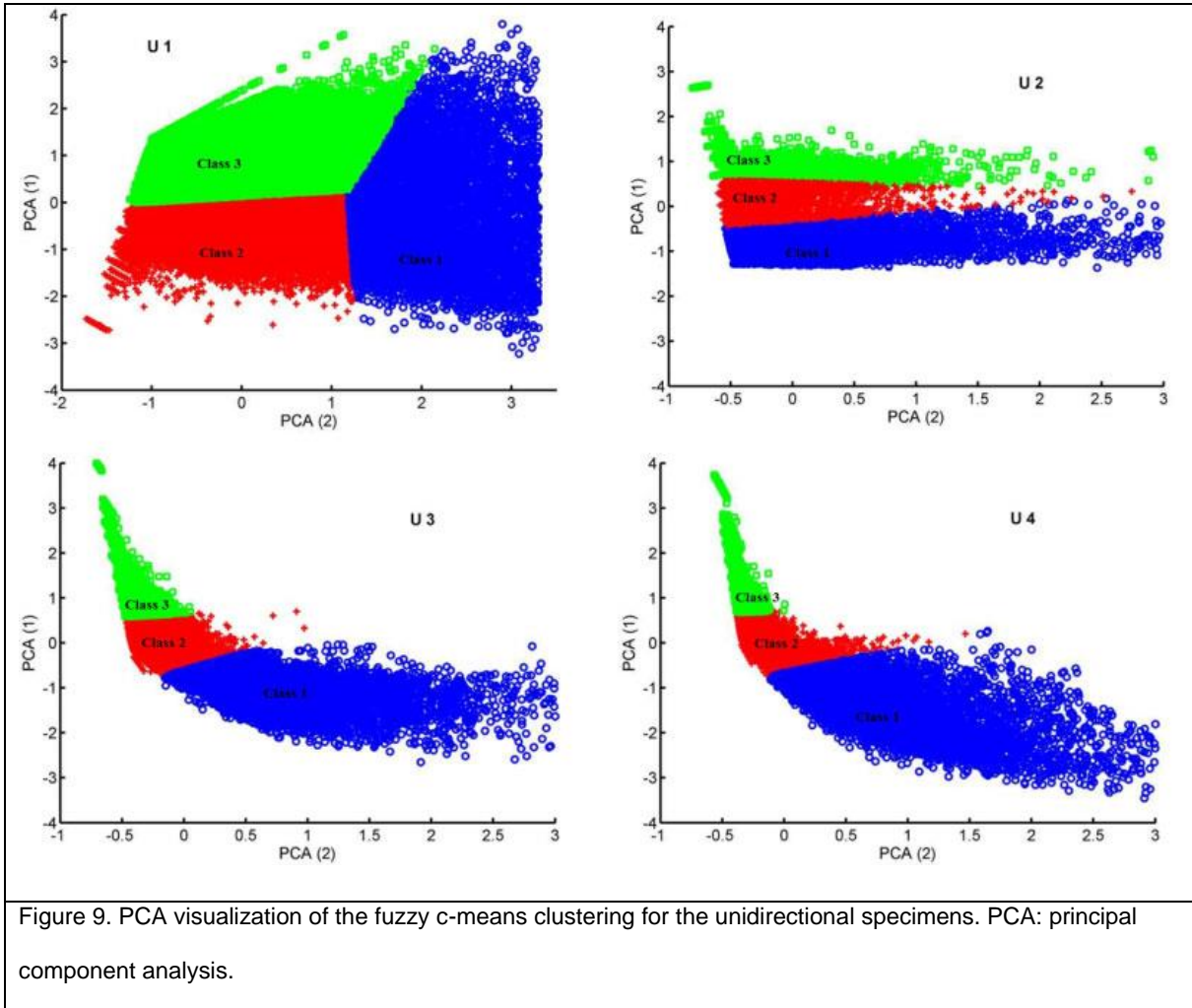
Figure 9. PCA visualization of the fuzzy c-means clustering for the unidirectional specimens. PCA: principal component analysis.
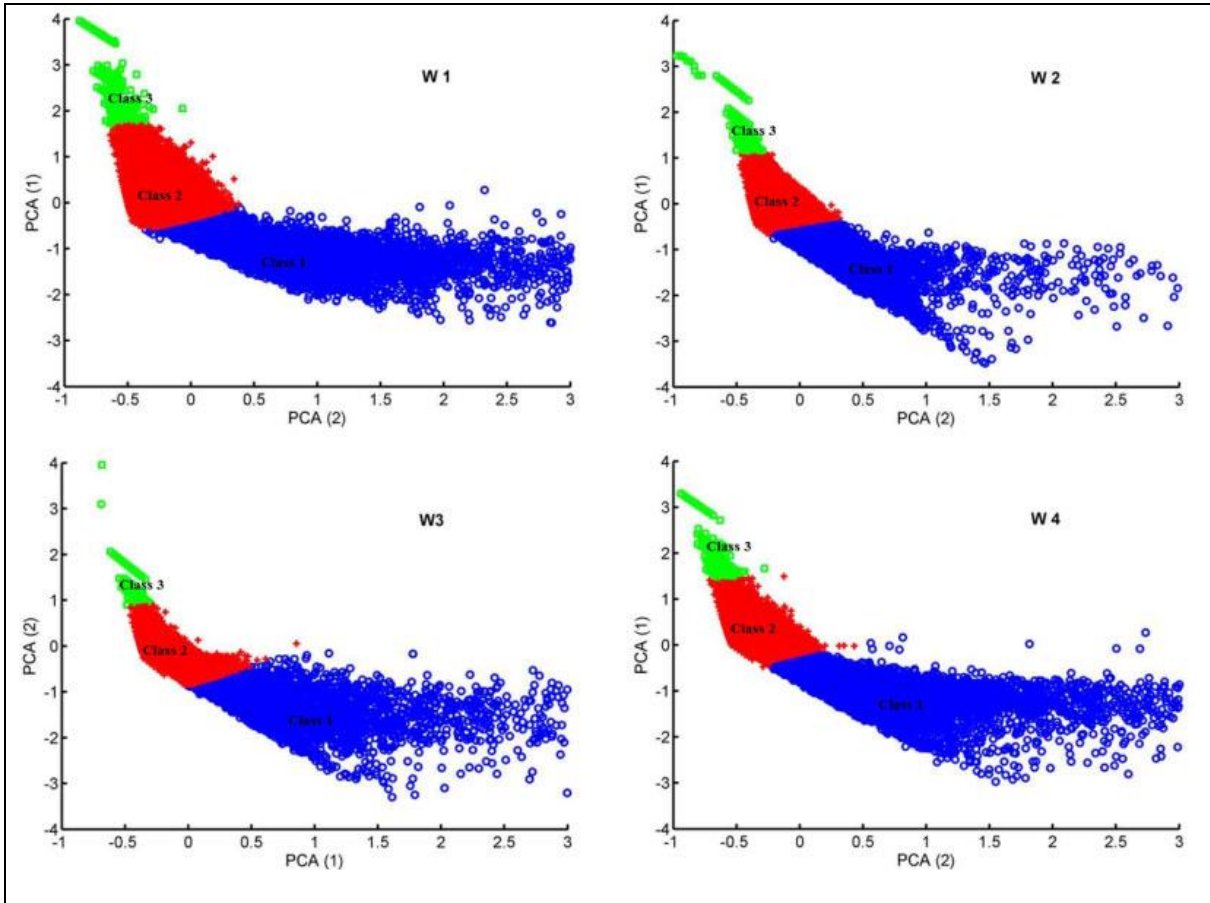
Figure 10. PCA visualization of the fuzzy c-means clustering for the woven specimens. PCA: principal component analysis.

The FCM results show that the AE signals are well separated along the first principal direction and are clustered in three different classes. The number of clusters was chosen based on SEM observation from the fractured surfaces and was also verified by Davis-

Bouldin (DB) index validity criterion. It is also noticeable that the distribution of the classes does not overlap (see Table 3).

Table 3. Average dependency percentage of the signals for three classes.

Name	Dependency percentage on the first class	Dependency percentage on the second class	Dependency percentage on the third class
U1	34	30	36
U2	40	35	25
U3	55	23	22
U4	60	30	10
W1	49	38	13
W2	51	37	12
W3	53	37	10
W4	65	27	8

Moreover, it can be observed from Table 3 that the AE signals distribution percentage at each cluster varies from one experimental condition to another. By considering the AE parameters of the obtained classes, the frequency parameter was best distinguished. The frequency range for each cluster is obtained confirming that the proposed method is useful for data clustering and damage mechanism detection. The distributions of the clustered AE events and the order of the AE events appearance are shown in Figures 11 and 12 for specimens U1 and W1, respectively. These Figures highlight three separate frequency

ranges for these specimens. The lower band frequency class (class1) is the earliest damage mode that appears in the tests.
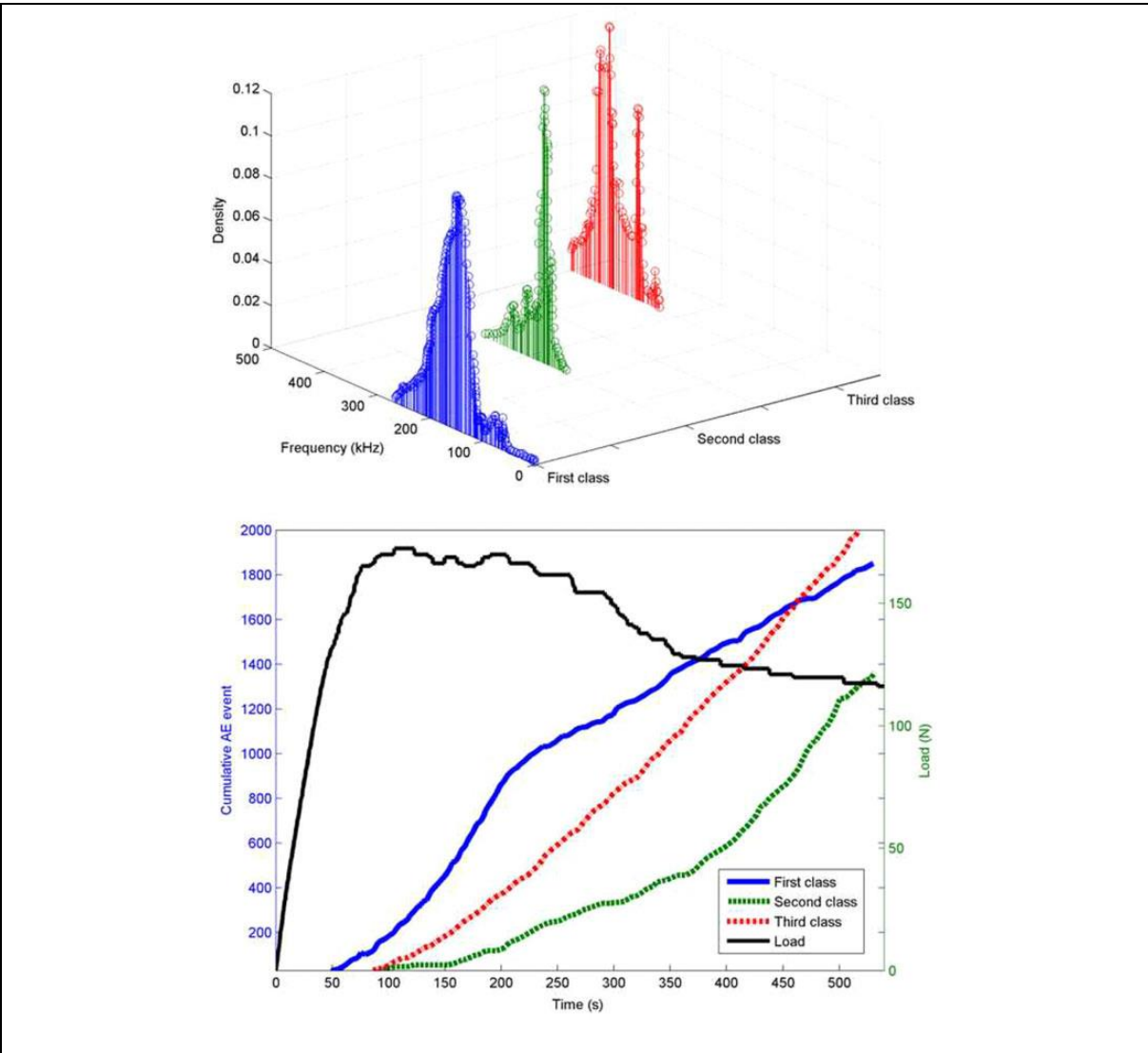

Figure 11. Frequency distribution and sequence of the classified signals versus load–displacement belonging to specimen U1.
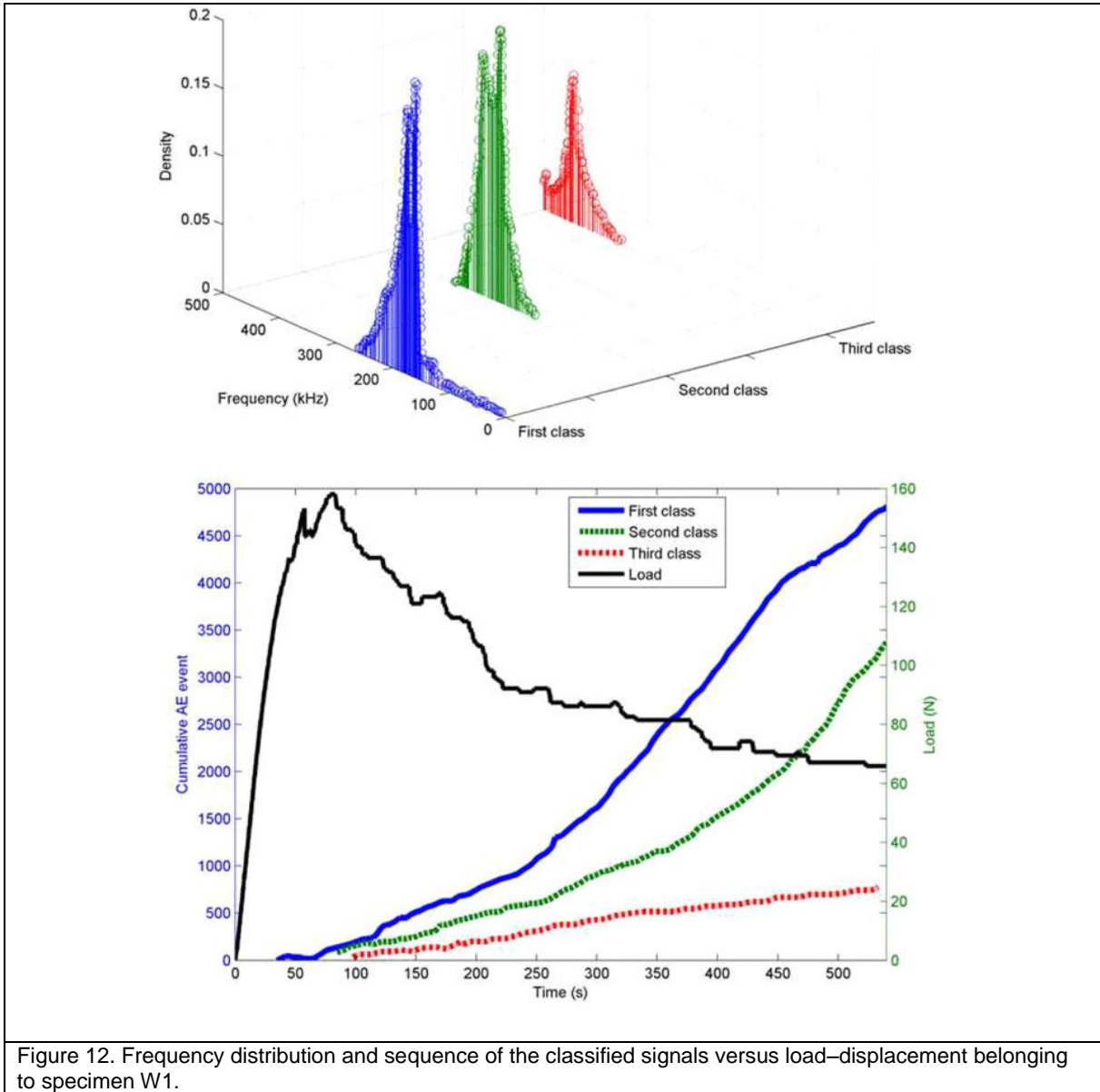
Figure 12. Frequency distribution and sequence of the classified signals versus load–displacement belonging to specimen W1.

Assigning AE features to the damage mechanisms

According to the previous referenced studies, matrix cracking, fiber-matrix debonding and fiber breakage are three prevalent damage mechanisms in delamination of glass/epoxy composite laminates. These different failure mechanisms are related to the crack tip condition. Different loading conditions and layup variation are the main cause of diversity in the form and radius of the crack tip area, resulting in different stress concentrations in each test condition. Consequently, dissimilar viscoelastic stress relaxation processes appear in the specimens. These dissimilar processes are the cause for diversity of frequency range in different fracture mechanisms. Bohse [31] expressed that intrinsic frequencies (f_i) are related to elastic acoustic velocity (c_i), relaxation time (τ_i), elastic module (E_i) and density (ρ_i) according to Equation 14.

$$f_i \sim \frac{1}{\tau_i} \sim c_i \sim \sqrt{\frac{E_i}{\rho_i}} \tag{14}$$

The relaxation time in the matrix/fiber interface differs for various damage mechanisms. Some studies showed that matrix cracking generates lower wide-band frequencies than fiber/matrix debonding and fiber breakage while the frequency range of fiber breakage is the highest. Furthemore, the frequency ranges of pure epoxy resin and glass fiber bundle

under tensile load were investigated and the results indicated that the dominant frequency ranges of the matrix cracking, debonding and fiber breakage are at 140–250 kHz, 250– 350 kHz and 350–450 kHz, respectively [9, 28, 32, 33].

Therefore, owing to the results of FCM clustering and WPT decomposition, the AE events and damage mechanisms could be related to each other. As a result, it can be concluded that the AE signals of the LHH3 component and the first FCM class are associated with matrix cracking damage, while the AE signals of the HLL3 component and second FCM class are representatives of fiber-matrix debonding damage. The AE signals of the HHL3 component and third FCM class are also related to the fiber breakage damage. In the case of specimen U1, U2 and U3, fiber bridging event and resistance of the fibers against crack opening occurs after initiation of the delamination (see Figure 13). However, in specimen U4 and the woven specimens, fiber bridging event is not observed by visual inspection.
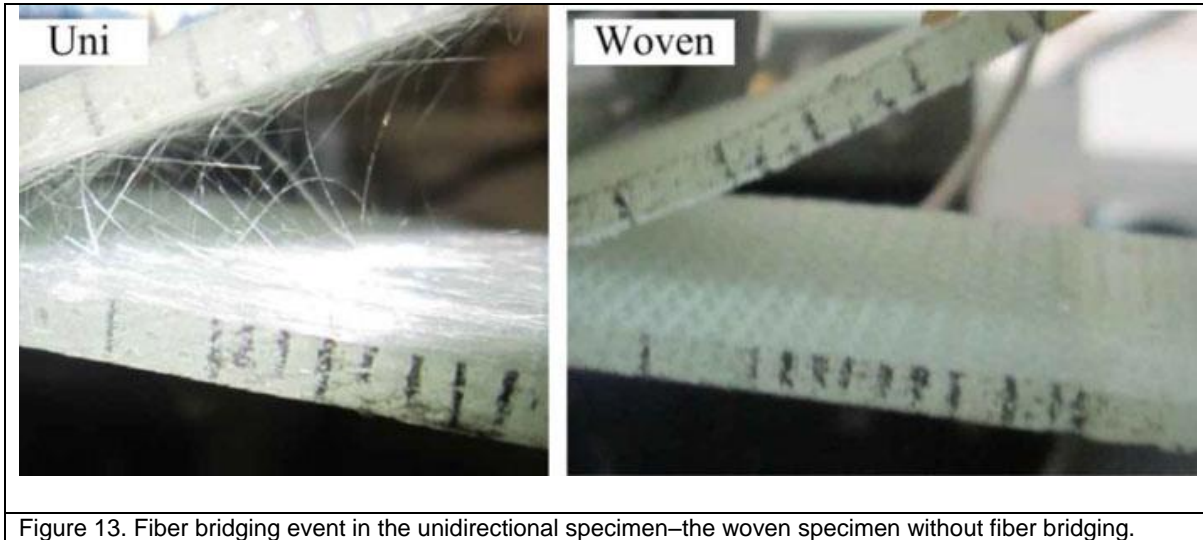
Figure 13. Fiber bridging event in the unidirectional specimen–the woven specimen without fiber bridging.

According to the FCM and WPT results, the percentage of the fiber breakage in the unidirectional specimens and mode I condition is higher than the woven specimens.

By increasing contribution of mode II, the percentage of fiber breakage diminishes in specimens U2, U3, W2 and W3 (see Tables 2 and 3). In these loading conditions, matrix cracking and fiber-matrix debonding are the most significant damage mechanisms in the specimens, whereas fiber breakage is not significant. It is also found that matrix cracking is the earliest damage mode that appears from the beginning of the tests, while debonding and fiber breakage take place later.

It should be mentioned that there are some AE events in the WPT and PCA results with frequency ranges unrelated to the frequency ranges of matrix cracking, debonding and fiber

breakage. These AE events should be associated with some other phenomena. The percentage of these AE events is small compared to the dominant damage mechanisms. In addition, other conditions like crack jumping from one layer to another one and other factors such as imperfections in the specimens and inappropriate teflon insert are the main factors affecting the obtained results.

Fractography

Figures 14 to 17 show delaminated surfaces of specimens U1, W1, U4 and W4. The SEM observations show that fracture mechanisms of the investigated specimens are a mixture of matrix cracking, fiber matrix debonding and fiber breakage. The quantities of these damage mechanisms are different from one specimen to another. Different interface lay-ups and different GII/GT modal ratio values are the main reason for this diversity. In the unidirectional specimens and near mode I conditions, the fibers being pulled away, resist against crack opening, until they broke (fiber bridging event). Therefore, as can be clearly observed from Figure 17, the highest fraction of fiber breakage appears in the case of specimen U1.

By increasing modal ratio value in the unidirectional and woven specimens, few fiber breakages were detected and the most damage mechanisms were observed in the resin and

at the interface of the fiber and matrix. The highest fraction of matrix cracking and fiber/matrix debonding occurs in the woven specimens and mode II condition. In addition, in the woven lay-ups, fiber breakage damage is rarely observed in all the loading conditions which may be related to the lack of fiber bridging event.
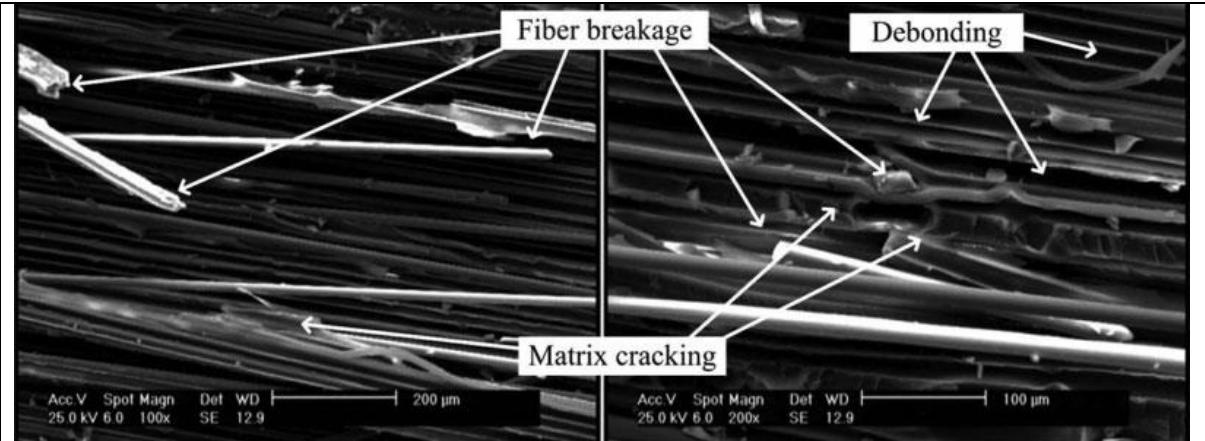

Figure 14. SEM observations for specimen U1. SEM: scanning electron microscopy.
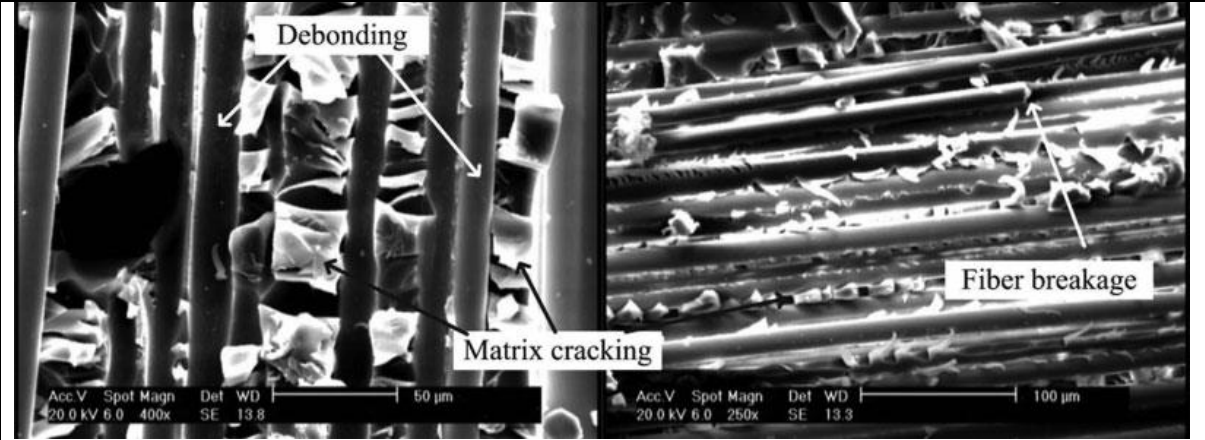
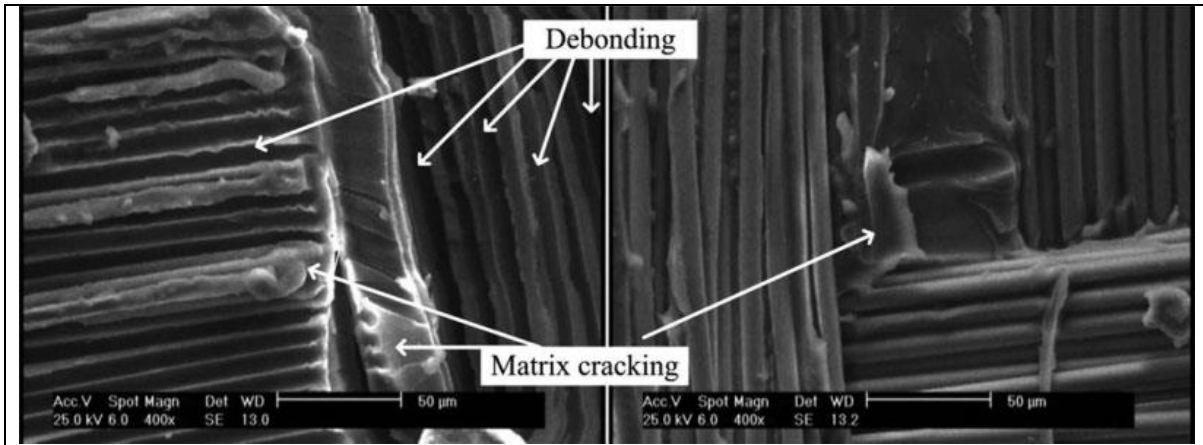Figure 15. SEM observations for specimen U4. SEM: scanning electron microscopy.

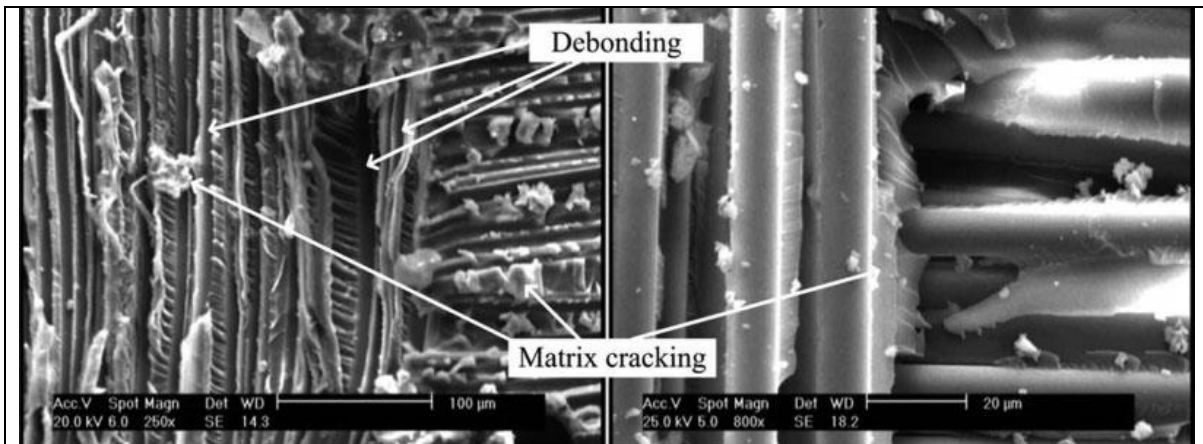Figure 16. SEM observations for specimen W1. SEM: scanning electron microscopy.

Figure 17. SEM observations for specimen W4. SEM: scanning electron microscopy.

Concluding remarks

In this work, multivariable analysis is applied to discriminate the damage mechanisms of glass/epoxy composites in actual occurring modes of delamination damage according to their AE patterns. Discrimination of the AE events was accomplished using WPT and FCM associated with a PCA. In WPT, the AE signals were decomposed into three levels and the energy distribution criterion was then employed to find the dominant components from the energy criterion point of view. By performing PCA clustering analysis on the AE data, three clusters with separate frequency ranges were obtained. The frequency range of the resulting clusters and components were then correlated to the damage mechanisms. Based on the different visco-elastic relaxation processes and the obtained results, the dominant frequency range of the signals for matrix cracking is at a lower level than the dominant frequency range of fiber bundle breakage. The frequency range for debonding is also considered between the fiber and matrix interfaces. Therefore, it was found that the AE signals of the three clusters and the dominant components were representative of the matrix cracking, fiber-matrix debonding and fiber breakage, respectively.

According to the distribution of the AE signals in different clusters, different AE signatures were noted between the different interface types and different GII/GT modal ratio values. The results showed that the percentage of the fiber breakage in the

unidirectional specimens and mode I condition is higher than those in the woven specimens and mode II. Additionally, matrix cracking and fiber-matrix debonding are the dominant damage mechanisms in all the specimens. The SEM observations revealed that the damage mechanisms of matrix cracking, debonding and fiber breakage were the sources of the AE signals. Therefore, it was concluded that the presented methods were successful in the classification process to improve the characterization of the damage mechanisms in actual occurring modes of delamination, i.e. mode I, mode II and the combination of these pure modes.

Acknowledgements

References

[1] Paris I and Poursartip A. Delamination Crack Tip Behavior at Failure in Composite Laminates under Mode I Loading. J Thermoplast Compos Mater 1998; 11(1): 57-69.

[2] Fotouhi M and Ahmadi M. Acoustic emission-based study to characterize the initiation of delamination in composite materials. J Thermoplast Compos Mater 2014. DOI: 10.1177/0892705713519811.

[3] ASTM E 569-97: 1998. Standard practice for acoustic emission monitoring of structures during controlled stimulation.

[4] Clough RB and McDoriough WG. The Measurement of Fiber Strength Parameters in Fragmentation Tests by Using Acoustic Emission. Compos Sci Technol 1996; 56(10): 1119-1127.

[5] Guerjouma REl, Baboux JC, Ducret D, et al. Nondestructive evaluation of damage and failure of fiber reinforced polymer composites using ultrasonic waves and acoustic emission. Adv Eng Mater 2001; 3: 601–608.

[6] Ramirez-Jimenez CR, Papadakis N, Reynolds N, et al. Identification of failure modes in glass/polypropylene composites by means of the primary frequency content of the acoustic emission event. Compos Sci Technol 2004; 64: 1819–1827.

[7] Barre S and Benzeggagh ML. On the use of acoustic emission to investigate damage mechanisms in glass-fiber reinforced polypropylene. Compos Sci Technol 1994; 52: 369–376.

[8] Fotouhi M, Pashmforoush F, Ahmadi M, et al. Monitoring the initiation and growth of delamination in composite materials using acoustic emission under quasi-static three-point bending test. J Reinf Plast Compos 2011; 30: 1481-1493.

[9] Refahi Oskouei A and Ahmadi M. Fracture Strength Distribution in E-Glass Fiber Using Acoustic Emission. J Comp Mater 2010; 44: 693-705.

[10] Fotouhi M and Najafabadi MA. Investigation of the mixed-mode delamination in polymer-matrix composites using acoustic emission technique. J reinf plast compos 2014; 33: 1767-1782.

[11] Benmedakhene S, Kenane M and Benzeggagh ML. Initiation and growth of delamination in glass/epoxy composites subjected to static and dynamic loading by acoustic emission monitoring. Compos Sci Technol 1999; 59: 201–208.

[12] Siron O, Chollon G, Tsuda H, et al. Microstructural and mechanical properties of filler-added coal-tar pitch-based C/C composites: the damage and fracture process in correlation with AE waveform parameters. Carbon 2001; 39: 2065–2075.

[13] Philippidis TP, Nikolaidis VN and Anastassopoulos AA. Damage characterization of carbon/carbon laminates using neural network techniques on AE signals. NDT&E Int 1998; 31: 329–340.

[14] Haykin S. Neural networks: A comprehensive foundation. 2th ed. New York: Macmillan College, 1994.

[15] Suresh S, Omkar SN, Mani V, et al. Classification of acoustic emission signal sources using genetic programming. Int J Aerospace Sci Technol 2004; 56: 26–40.

[16] Godin N, Huguet S and Gaertner R. Integration of the Kohonen's self-organising map and K-means algorithm for the segmentation of the AE data collected during tensile tests on cross-ply composites. NDT&E Int 2005; 38: 299–309.

[17] Minak G, Morelli P and Zucchelli A. Fatigue residual strength of circular laminate graphite–epoxy composite plates damaged by transverse load. Comp Sci Technol 2009; 69(9): 1358–1363.

[18] Oskouei AR, Zucchelli A, Ahmadi M, et al. An integrated approach based on acoustic emission and mechanical information to evaluate the delamination fracture toughness at mode I in composite laminate. Mater Des 2011; 32: 1444–1455.

[19] Marec A, Thomas JH and Guerjouma El. Damage characterization of polymer-based composite materials: multivariable analysis and wavelet transform for clustering acoustic emission data. Mech Syst Signal Process 2008; 22: 1441–1464.

[20] Yuan X and Li Z. Tool wear monitoring with wavelet packet transform- fuzzy clustering method. Wear 1998; 219: 145–154.

[21] Omkar SN, Suresh S, Raghavendra TR, et al. Acoustic emission signal classification using fuzzy C-means clustering. In: Proceedings of the 9th international conference on neural information processing (ICONIP02), Singapore, 2002, Vol. 4; IEEE; pp. 1827–1831.

[22] Oskouei AR, Heidary H, Ahmadi M, et al. Unsupervised acoustic emission data clustering for the analysis of damage mechanisms in glass/polyester composites. Mater Des 2012; 37: 416–422.

[23] Ni QQ and Iwamoto M. Wavelet Transform of Acoustic Emission Signals in Failure of Model Composites, Eng Fract Mech 2002; 69(6): 717–728.

[24] Velayudham A, Krishnamurthy R and Soundarapandian T. Acoustic emission based drill condition monitoring during drilling of glass/phenolic polymeric composite using wavelet packet transform. Mater Sci Eng A 2005; 412: 141–145.

[25] Rao RM and Bopardikar AS. Wavelet transforms introduction to theory and applications. Amsterdam: Addison- Wesley, 1998.

[26] Wojtaszczyk P. A mathematical introduction to wavelets. London: Cambridge University Press, 1997.

[27] Soman KP and Ramachandran KI. Insight into wavelets from theory to practice. India: Prentice-Hall, 2004.

[28] Refahi OA, Ahmadi M and Hajikhani M. Waveletbased acoustic emission characterization of damage mechanism in composite materials under mode I delamination at different interfaces. Exp Polym Lett 2009; 3: 804–813.

[29] Oja E. Neural networks: principal components and subspaces. Int J Neural Syst 1989; 1: 61–68.

[30] Sadaaki M. Information clustering based on fuzzy multisets. Inf Process Manage 2003; 39: 195–213.

[31] Bohse J. Acoustic emission characteristics of micro-failure processes in polymer blends and composites. Compos Sci Technol 2000; 60: 1213–1226.

[32] Pashmforoush F, Fotouhi M and Ahmadi M. Damage characterization of glass/epoxy composite under three-point bending test using acoustic emission technique. J Mater Eng Perform 2012; 21(7): 1380-1390.

[33] Fotouhi M., Saeedifar M., Sadeghi S., Ahmadi M., Minak G. Investigation of the damage mechanisms for mode I delamination growth in foam core sandwich composites using Acoustic Emission, J Structural Health Monitoring, 2015, DOI: 10.1177/1475921714568403.

List of Figure captions

Figure 1. The procedure for damage recognition.

Figure 2. The specimen geometry and dimension.

Figure 3. Experimental setups for loading and the AE sensors. (a: mode I, b: Mode II and c:Mixed-mode).

Figure 4. WPT tree. Letter L refers to Low frequency and letter H refers to High frequency.

Figure 5. The load/time curves and AE energy distribution for the unidirectional specimens.

Figure 6. The load/time curves and AE energy distribution for the woven specimens.

Figure 7. Waveforms of specimen U1 obtained from different regions.

Figure 8. Energy percentage of each component of the 3rd level in time domain calculated for different specimens.

Figure 9. PCA visualization of the fuzzy c-means clustering for the unidirectional specimens.

Figure 10. PCA visualization of the fuzzy c-means clustering for the woven specimens.

Figure 11. Frequency distribution and sequence of the classified signals versus load-displacement belonging to specimen U1.

Figure 12. Frequency distribution and sequence of the classified signals versus load-displacement belonging to specimen W1.

Figure 13. Fiber bridging event in the unidirectional specimen- the Woven specimen without fiber bridging.

Figure 14. SEM observations for specimen U1.

Figure 15. SEM observations for specimen U4.

Figure 16. SEM observations for specimen W1.

Figure 17. SEM observations for specimen W4.

List of Table captions

 Table 1. specification of the investigated lay-ups.

Table 2. Summary of wavelet packet analysis for dominant components.

Table 3. Average dependency percentage of the signals for three classes.